Damage Assessment of Reinforced Concrete Shear Walls by Acoustic Emission

Alireza Farhidzadeh[1], Salvatore Salamone[2], Ehsan Dehgghan-Niri[3], Bismarck Luna[4] and Andrew Whittaker[5]

[1,2,3,4,5]State University of New York at Buffalo
[1,2,3]Smart Structures Research Laboratory (SSRL), Department of Civil, Structural, and Environmental Engineering, State University of New York at Buffalo, 212 Ketter Hall, Buffalo, NY, 14260
[1](716) 868-9852; e-mail alirezaf@buffalo.edu
[2](716) 352-9848; fax (716) 645-3667; e-mail: ssalamon@buffalo.edu
[3](716) 645-5403; e-mail ehsandeh@buffalo.edu

[4,5]Structural Engineering and Earthquake Simulation Laboratory (SEESL), Department of Civil, Structural, and Environmental Engineering, State University of New York at Buffalo, 212 Ketter Hall, Buffalo, NY, 14260
[4](716) 645-5403; e-mail bismarck@buffalo.edu
[5](716) 645-4364; fax (716) 645-3667; e-mail awhittak@buffalo.edu

Abstract

Reinforced concrete (RC) shear walls are popular structural systems to resist lateral forces like wind and earthquake. The cracking behavior of these critical structural elements is crucial due to its harmful effects on structural performance such as serviceability and durability requirements. A technique that shows promise for monitoring RC structures is acoustic emission (AE). This paper presents an experimental investigation of fracture processes of two large-scale RC shear using AE parameters. In addition, a novel cluster analysis based on the k-means is presented to automatically classify the two fundamental cracks modes (i.e., tensile and shear).

Keywords: acoustic emission, *b*-value analysis, reinforced concrete shear wall, crack classification, *k*-mean

INTRODUCTION

Reinforced concrete (RC) shear walls are widely used in conventional building and safety-related nuclear structures. They provide much or all of a structure's lateral strength and stiffness to resist earthquake and wind loadings. The cracking behavior of these critical structural elements is crucial due to its harmful effects on structural performance such as serviceability and durability requirements. In the past two decades, significant efforts have been made toward the development of structural health monitoring (SHM) systems in order to reduce life-cycle costs and improve safety of civil infrastructures. A technique that shows promise for monitoring RC structures is acoustic emission (AE) (Aggelis 2011, Carpinteri et al. 2007, Kurz 2006). In general, AE are stress waves caused by sudden strain releases due to internal fracture such as concrete cracking (Grosse and M. Ohtsu 2008). Extracting features from the AE signal is usually referred to as parameter-based technique. Figure 1 shows a typical AE signal with the most common features used during an AE testing (i.e., peak amplitude, rise-time, duration, and count). A threshold is set somewhat above the background level and serves as a reference for the waveform features. The AE peak amplitude is defined at the maximum amplitude of the signal. The number of times the signal rises and crosses the threshold is the count of the AE event. The time period between the rising edge of the first count and the falling edge of the last count is the duration of the AE event. Finally, the time period between the rising edge of the first count and the peak of the AE event is defined to be the rise time. This paper presents results of an AE monitoring of two large-scale RC shear walls (SW1 and SW2) subjected to cyclic loading. Some features were extracted from the AE signals to perform the critical tasks of: 1) crack propagation monitoring and 2) crack classification. In particular, one of the most important AE parameters, that is, the *b*-value has been used to monitor the crack propagation (Farhidzadeh et al. 2012a, under review) whereas a cluster analysis, based on the *k*-mean, has been used to perform a crack classification (Farhidzadeh et al. 2012b, under review). This paper is organized as follow: section 2 provides a brief overview of the *b*-value analysis and Gaussian filtering. The crack classification procedure based on *k*-mean analysis is then described in section 3. Section 4 describes the experimental setup followed by the results in section 5.

b-VALUE ANALYSIS

The *m*-value is obtained using the frequency–magnitude distribution data by means of Gutenberg–Richter relationship, which is generally used in seismology. The Gutenberg–Richter (1949) formula in terms of AE technique is as follow:

$$logN(A_{dB}) = a - b(A_{dB}/20) \tag{1}$$

where $N(A_{dB})$ is the incremental frequency (i.e. the number of AE events with amplitude greater than the A_{dB}), a is an empirical constant, b is the b-value, and A_{dB} is the peak amplitude of AE event in decibel. The b-value analysis of AE signals is in general applied to a certain number n of AE signals. Suggested values of n found in literature range from 50 to 100 (Shiotani et al. 2001). Several studies have shown that during the process of fracture of an RC specimen there is a relationship between the b-value and types of cracks. In general, the b-value increases during the formation of micro-cracks (i.e., early stages of damages) and decreases when the macro-cracks begin to localize (Colombo et al. 2003). Although b-value analysis show promise in monitoring the dynamics of cracks, only few if any such methods have been transitioned to field applications. A reason, for this lack of acceptance are the highly fluctuations of the b-value caused by the normal operating condition of the structure, which make extremely difficult interpreting the results. To overcome this limitation a Gaussian filter is proposed in this work.

Gaussian Filter

Gaussian functions have the following properties that make them particularly useful in smoothing filters (Lin et. al 1996): (1) The gaussian function is symmetric about the mean, and the weights assigned to signal values decrease gradually with distance from the mean. (2) The width of the gaussian function is determined by its spread parameter, i.e., the standard deviation. (3) The local extrema (e.g. b-value drop) observed at one standard deviation are also observable at the smaller standard deviations and no more local extrema are created as the spread parameter increases. Gaussian smoothing is literally the convolution of a gaussian window and a 1D vector of data. The Gaussian smoothing $F(x)$ of a one-dimentional signal, $f(x)$, is defined as:

$$F(x) = f(x) * g(x,\sigma) = \int_{-\infty}^{\infty} f(\mu)\, g(x-\mu,\sigma)\, d\mu = \int_{-\infty}^{\infty} f(\mu) \frac{1}{\sqrt{2\pi}\sigma} \exp\left[-\frac{(x-\mu)^2}{2\sigma^2}\right] d\mu \tag{2}$$

where "*" denotes convolution with respect to x, $g(x,\sigma)$ is the gaussian function with the standard deviation σ, and μ is a dummy variable. These filtering parameters in addition to window span should be properly selected to clarify the trend. Example of a local extrema (i.e., b-value drop caused by loading) is shown in Figure 1. A uniform smoothing can eliminate this local drop, depend on window span, but gaussian smoothing will maintain it because it gives more weight to window center and less to the tails.

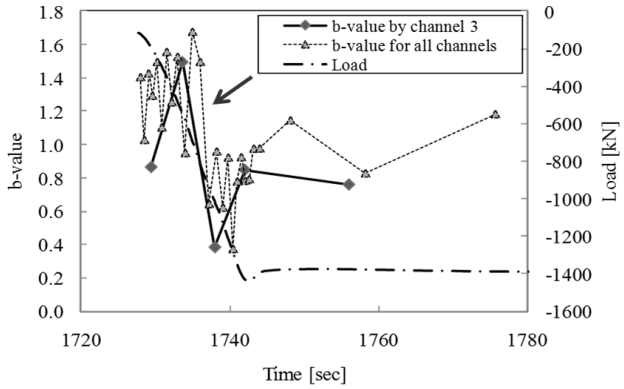

Figure 1: Local drop in *b*-value as a result of loading.

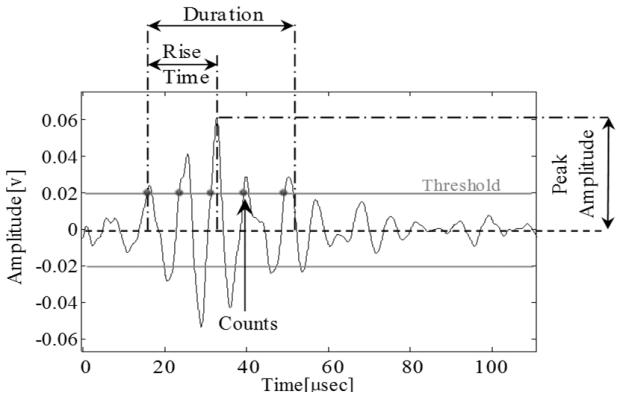

Figure 2: Acoustic emission signal with features.

CRACK CLASSIFICATION

In the last two decades several efforts have been made to correlate AE features with the cracking mode in RC members, which adversely affects structural performance in various ways such as durability and serviceability. Ohno and Ohtsu (2010) proposed a technique to perform crack mode classification in concrete structures based on two AE parameters, namely: "average frequency (AF)" and the "RA" value, which are defined as (see Figure 2):

$$RA = (Rise\ time) / (Peak\ Amplitude) \tag{3}$$

$$Average\ Frequency = (AE\ ring\text{-}down\ count) / Duration \tag{4}$$

Cracks will be categorized as Figure 3 illustrates. However, a defined criterion (i.e., the inclined line) on the proportion of the RA value and the average frequency for crack classification has not been confirmed yet (Ohno and Ohtsu 2010). In this work, a *k*-means pattern recognition method is utilized to classify the AE events in two dominant shear and tensile groups.

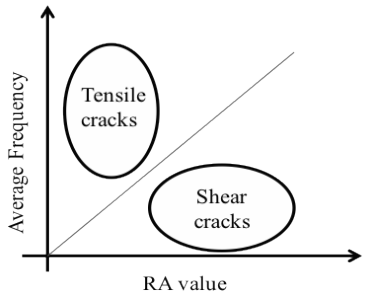

Figure 3: Signal classification based upon JCMS-IIIB5706 code.

k-mean Clustering

This method aims at partitioning the data sets into k disjoint subsets (clusters) based on minimizing the summation of square distance of each data point in a subset to the center of the subset in which it is partitioned (Likas et al. 2003). Indeed, several studies based on pattern recognition of AE events have determined that it is feasible to distinguish efficiently the events associated with various failure mechanisms. Suppose that a data set $X=\{x_1, x_2,\ldots x_N\}$, $xn \in R^d$, is available. *k*-means aims at partitioning this data sets into *k* disjoint subsets, $C_1, \ldots, C_k$, through minimizing the criterion or clustering error as follow

$$E(m_1, m_2, ..., m_k) = \sum_{i=1}^{N} \sum_{j=1}^{k} I(x_i \in C_j) \left\| x_i - m_j \right\|^2 \tag{5}$$

where m_j is the center of j^{th} cluster, C_j, and $I(P)$=1 if P is true and 0 otherwise. This criterion can be minimized through iterative procedure summarized in the following steps: 1) Initializing *k* centers,$\{m_1,\ldots, m_k\}$, through randomly dividing the data set into *k* groups and calculating the mean value for each subset. 2) Assigning each data point, x_n, to a cluster, C_j , that its center, m_j, has the lowest Euclidean distance to the point among other cluster centers. 3) Re-computing the centers for *k* clusters, $\{m_1,\ldots, m_k\}$. 4) If the change in centers in two proceeding steps is less than a certain threshold then algorithm is converged and terminate the iteration; otherwise go to step 2.

EXPERIMENTAL SETUP

The test specimens were two large scale RC shear walls, SW1 and SW2, with the thickness of 0.2 m, width of 3.05 m and height to width ratio of 0.94 and 0.54, respectively. More details about the design of these walls are available in (Rocks 2012). The main components of the AE system included an eight-channel high-speed data acquisition board (Physical Acoustics Corporation Micro-II PAC) and AEwin software for signal processing and storage. SW1 was instrumented with eight R15α AE sensors whereas SW2 with four R15α and four R6α. Sensors were attached to one face of the wall using hot glue. Preamplifiers were set at 40 dB gain and analog bandpass filters were adjusted in the interval of 20 kHz to 400 kHz. Trigger levels of 35 dB and 48 dB were selected to remove the background noise for SW1 and SW2, respectively. The sensor layout used for the two specimens is shown in Figure 4.

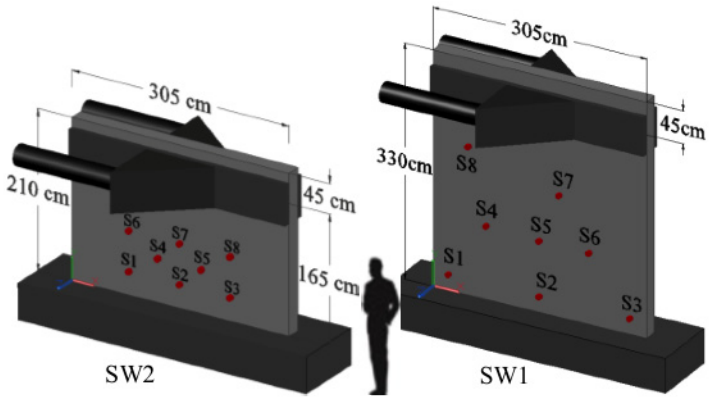

Figure 4: RC wall, load actuators, dimensions, and sensor layout for SW1 and SW2.

Attenuation measurements were carried out by pencil lead breaks made at the center of the specimen, as shown in Figure 5. A circular array of AE sensors (R15α from Mistras) were used to estimate the attenuation coefficient in different directions, as shown in Figure 5(a). Figure 5(b) shows the topography of the AE amplitudes obtained in the SW1. It can be observed that larger amplitudes were observed in the horizontal direction rather than the vertical one. Non-homogeneity and rebar directions of reinforced concrete are the main reason for not having smooth attenuation boundaries. The variation range of the attenuation coefficient for the SW1 was between 20 dB/m to 40 dB/m with an average of 34.7 dB/m. This average was 29.6 dB/m for the SW2.

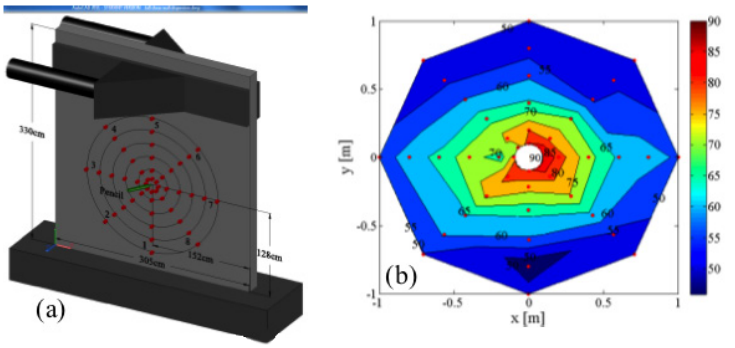

Figure 5: (a)AE sensor layout for attenuation measurements in SW1;
(b)topography of AE peak amplitude due to pencil lead breaks at the center.

Table 1 summarizes the coordinates of sensors for loading experiment. The in-plane quasi-static reversed cyclic loading protocol consisted of 10 load steps (LS) starting from LS1 to LS10 for SW1 and 10 load steps starting from LS2 to LS11 for SW2. Each load step consists of two cycles. The force-displacement hysteresis loops and their corresponding backbone (Farhidzadeh et al. 2012a,b; under review) show that onset of nonlinear behavior and maximum capacity were observed in LS7 and LS9 respectively, for SW1 whereas in LS8 and LS10 respectively, for SW2.

Table 1: Sensor coordinates.

Sensor		S1	S2	S3	S4	S5	S6	S7	S8
Coordinates [cm]	SW1	(23,23)	(157,23)	(281,23)	(77,103)	(157,103)	(228.103)	(183,156)	(50,183)
	SW2	(81,32)	(153,32)	(225,32)	(122,59)	(184,59)	(81,86)	(153,86)	(225,86)

EXPERIMENTAL RESULTS

To monitor the fracture process of both specimens during the test a *b*-value analysis was carried out as explained in section 2. In particular, the *b*-value was calculated using groups of n=70 AE signals. Figure 6 shows the *b*-value results obtained considering the entire dataset (i.e. *b*-values obtained using data collected by all sensors) without the filtering process, along with the corresponding probability density function. As can be seen in Figure 6, it is very difficult to identify a trend in the unfiltered *b*-value data; this difficulty most likely occurred because of the large amount of AE activity (mostly scattering effects) generated by the specimen under the cyclic loadings. A similar behavior was observed in SW1.

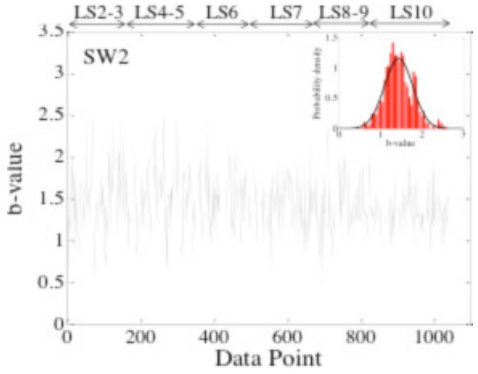

Figure 6: Unfiltered *b*-values data from SW2.

Figure 7 shows the results of the gaussian filtering applied to the *b*-value data for the two specimens. A dashed line is superimposed to highlight the overall *b*-value trend. It can be observed that an increasing *b*-value trend is followed by a plateau and then a decreasing trend.

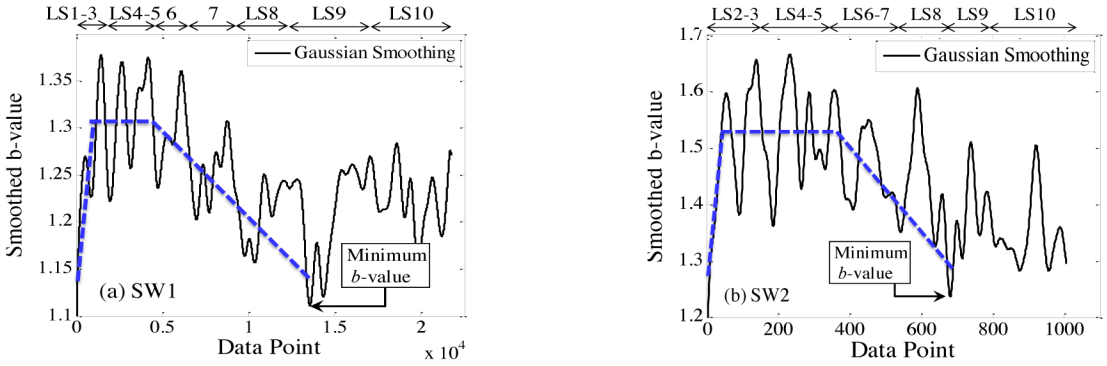

Figure 7: Filtered *b*-value for (a) SW1; (b) SW2.

We can infer that micro-cracks formation were dominant prior to LS3 (the increasing trend) and began to localize as macro-cracks prior to LS5 (plateau region). From this load step onward, *b*-values started to decrease (i.e., the macro-cracks opening). The decreasing trend began one load step prior to the yielding and reached to a minimum value at load step 9. Interestingly, both specimens reached to their maximum strength in the proximity of the load step 9. Figure 8 show the maximum and modal (most frequent) crack width in SW1. A similar crack propagation pattern

occurred in SW2. It can be observed that, the maximum crack width was less than 1 mm between LS1 and LS6. Although numerous cracks were formed in the specimen during these load steps, the crack widths did not change significantly. The maximum crack width recorded in the subsequent load steps increased up to 3 mm in LS7 and about 4 mm in LS9 as the specimen reached its maximum capacity. It should be noted there is an interest correlation between crack widths and *b*-values, that is, the *b*-value began to decrease at the load step in which the cracks widths increased. It can be concluded that a decreasing trend of the *b*-value may indicate an accumulation of damage in RC shear walls.

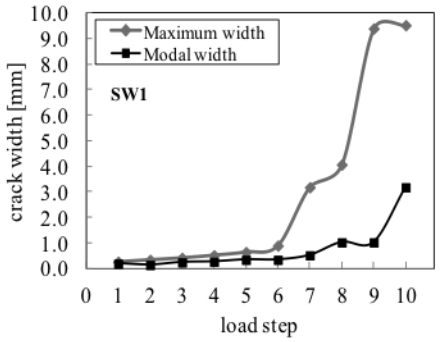

Figure 8: Maximum and modal crack widths, SW1 (Farhidzadeh et. al 2012b, under review).

Figure 9 and Figure 10 show smoothed *b*-value analysis results carried out on data recorded by some sensors for SW1 and SW2, respectively. The reducing trend and the corresponding load step confirm the conclusion obtained considering the data from all sensors.

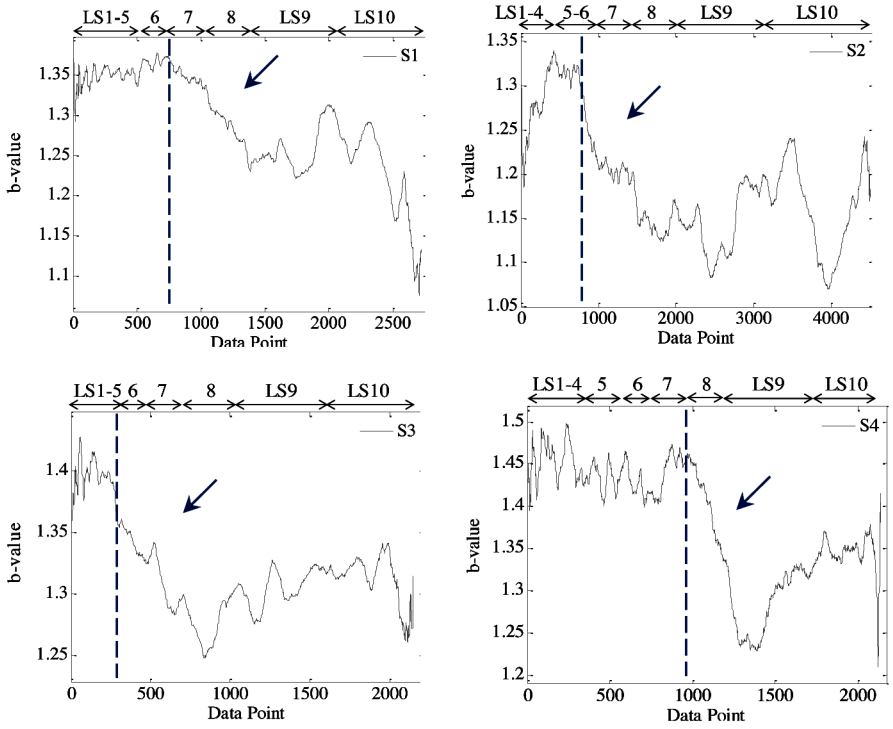

Figure 9: Sensor-based *b*-values for SW1 (Farhidzadeh et. al 2012b, under review).

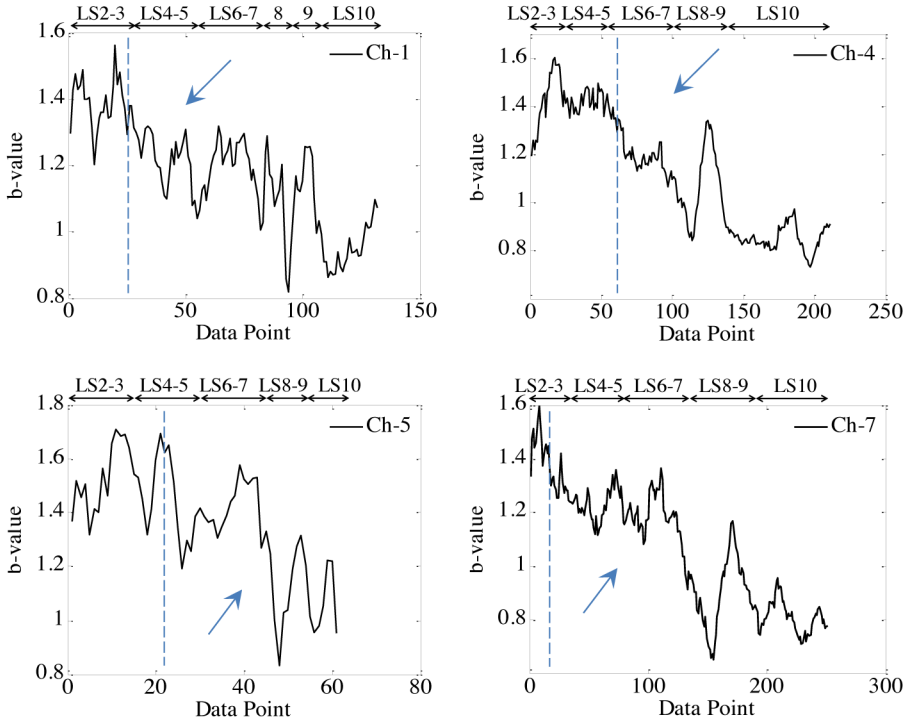

Figure 10: Sensor-based *b*-values for SW2.

In concrete structures, tensile cracks appear at low levels of loading while shear cracks appear in severe loading conditions. As expected, both diagonal shear and flexural cracks were formed in specimen SW1 due to its intermediate reinforcement ratio of 0.67% and relatively large aspect ratio of 0.94. In SW2, a small amount of horizontal flexural cracks were generated due to its relatively high reinforcement ratio of 1.0% and intermediate aspect ratio of 0.54. Therefore crack mode classification is more important to be investigated in SW1.

As discussed earlier, crack mode classification is done by *k*-mean clustering analysis for SW1. A moving average with window span of 70 hits carried out over the entire RA and AF values in each load step. The related results are presented in Figure 11. It shows that shear cracks become dominant after LS5 and grow quickly afterward. Visual inspection about the amount of horizontal and diagonal cracks confirmed such estimation (Farhidzadeh et. al 2012b, under review).

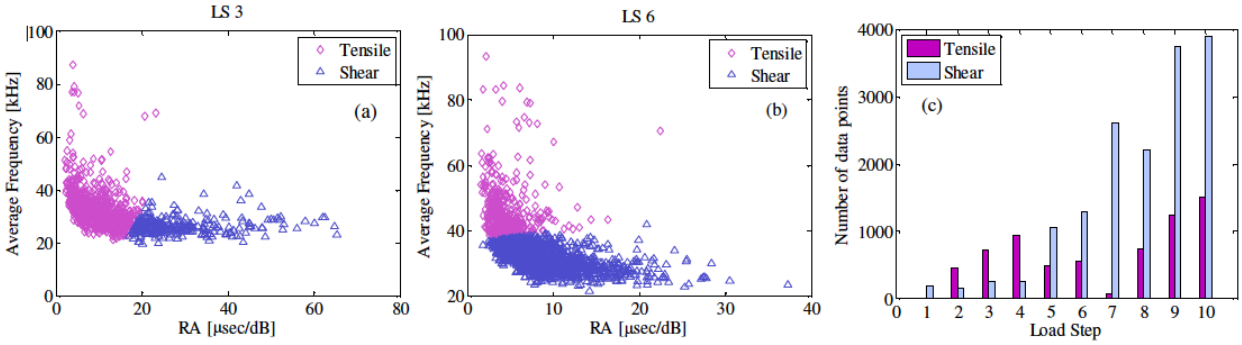

Figure 11. Crack mode classification for SW1 (a) in LS3; (b) in LS6;
(c) number of data points associated to tensile or shear mode for the entire experiment

CONCLUSIONS

Reinforced concrete (RC) shear walls are popular gravity and lateral force resisting systems. Failure of a shear wall could result in severe damage and even progressive collapse of a concrete structure. This paper described the monitoring of the fracture process of two large-scale RC shear walls subjected to cyclic loading using a sparse array of acoustic emission (AE) sensors. In particular, a *b*-value analysis was presented to monitor the crack propagation during the test. A gaussian filter was proposed to improve the interpretation of the *b*-value data. In addition, a cluster analysis based on the *k*-mean was used to automatically classify the two fundamental crack modes (i.e., tensile and shear).

ACKNOWLEDGMENTS

Authors acknowledge National Science Foundation (NSF) for providing the financial support on this project under Grant No. CMMI-0829978. The experiments presented herein could not have been completed without contributions from the staff of the Structural Engineering and Earthquake Simulation Laboratory (SEESL) of the State University of New York at Buffalo.

REFFERENCES

1. Aggelis, D.G. “Classification of cracking mode in concrete by acoustic emission parameters,” *Mechanics Research Communications*, 38(3), 153-157. 2011.
2. Carpinteri, A., G. Lacidogna, G. Niccolini and S. Puzzi. “Critical defect size distributions in concrete structures detected by the acoustic emission technique,” *Meccanica*, 43(3), 349-363. 2007.
3. Colombo, I.S., I.G. Main and M.C. Forde. “Assessing Damage of Reinforced Concrete Beam Using *b*-value Analysis of Acoustic Emission Signals,” *ASCE Journal of Materials in Civil Engineering*, 2003, 15(3), 280-286.
4. Farhidzadeh, A., S. Salamone, B. Luna and A. Whittaker. “Acoustic Emission Monitoring of a Reinforced Concrete Shear Wall by *b*-value based Outlier Analysis,” *Structural Health Monitoring–An International Journal*, under review. 2012a.
5. Farhidzadeh, A., E. Dehghan-Niri, S. Salamone, B. Luna and A. Whittaker. “Crack Propagation Monitoring in a Reinforced Concrete Shear Wall by Acoustic Emission,” *ASCE Journal of Structural Engineering*, under review. 2012b.
6. Grosse, C.U. and M. Ohtsu, “Acoustic Emission Testing – Basics for Research Applications in Civil Engineering,” *Berlin & Heidelberg*, Germany, Springer Verlag. 2008.
7. Gutenberg, B. and C.F. Richter. “Seismicity of the earth and associated phenomena,” *Frequency and Energy of Earthquakes*. Princeton, NJ, Princeton University Press, 17-19. 1949.
8. Kurz, J.H. “Stress Drop and Stress Redistribution in Concrete Quantified Over Time by the *b*-value Analysis,” *Structural Health Monitoring*, 5(1), 69-81. 2006.
9. Lin, H.C., L.L. Wang and S.N. Yang. “Automatic determination of the spread parameter in Gaussian smoothing,” *Pattern Recognition Letters*, 17(12), 1247-1252. 1996.
10. Likas, A., N. Vlassis and J. Verbeek. “The global k-means clustering algorithm,” *Pattern Recognition*, 36(2), 451-461. 2003.
11. Ohno, K. and M. Ohtsu. “Crack classification in concrete based on acoustic emission.” *Construction and Building Materials*, Elsevier Ltd, 24(12), 2339-2346. 2010.
12. Rocks, J.F. “Large Scale Testing of Low aspect Ratio Reinforced Concrete Walls” *M.Sc. Thesis*, Department of Civil, Structural and Environmental Engineering, University at Buffalo, NY. 2012.
13. Shiotani, T., S. Yuyama, Z.W. Li and M. Ohtsu. “Application of AE improved *b*-value to quantitative evaluation of fracture process in concrete materials,” *Journal of Acoustic Emission*, 19, 118-133. 2001.